Energy Storage Materials 20 (2019) 462–469

Contents lists available at ScienceDirect

Energy Storage Materials

journal homepage: www.elsevier.com/locate/ensm

Charge-transfer complexes for high-power organic rechargeable batteries

Sechan Lee [a], Jihyun Hong [b], Sung-Kyun Jung [a], Kyojin Ku [a], Giyun Kwon [a], Won Mo Seong [a], Hyungsub Kim [c], Gabin Yoon [a], Inyeong Kang [b], Kootak Hong [a], Ho Won Jang [a], Kisuk Kang [a,d,*,1]

[a] Department of Materials Science and Engineering, Research Institute of Advanced Materials (RIAM), Seoul National University, 1 Gwanak-ro, Gwanak-gu, Seoul 08826, Republic of Korea
[b] Center for Energy Materials Research, Korea Institute of Science and Technology (KIST), 5 Hwarang-ro 14 Gil, Seongbuk-gu, Seoul 02792, Republic of Korea
[c] Korea Atomic Energy Research Institute (KAERI), 111 Daedeok-daero 989 Beon-Gil, Yuseong-gu, Daejeon 34057, Republic of Korea
[d] Center for Nanoparticle Research, Institute for Basic Science (IBS), Seoul National University, 1 Gwanak-ro, Gwanak-gu, Seoul 08826, Republic of Korea

ARTICLE INFO

Keywords:
Organic rechargeable batteries
Charge-transfer complex
High power organic electrodes
Donor-acceptor complex
Novel organic electrode material candidates

ABSTRACT

Organic redox compounds are potential substitutes for transition-metal-oxide electrode materials in rechargeable batteries because of their low cost, minimal environmental footprint, and chemical diversity. However, their inherently low electrical conductivity and high solubility in organic solvents are serious impediments to achieving performance comparable to that of currently used inorganic-based electrode materials. Herein, we report organic charge-transfer complexes as a novel class of electrode materials with intrinsically high electrical conductivity and low solubility that can potentially overcome the chronic drawbacks associated with organic electrodes. The formation of the charge-transfer complexes, phenazine–7,7,8,8-tetracyanoquinodimethane and dibenzo-1,4-dioxin–7,7,8,8-tetracyanoquinodimethane, via a room-temperature process leads to enhancement in the electrical conductivity and reduction in the dissolution resulting in the high power and cycle performances that far outperform those of each single-moiety counterpart. This finding demonstrates the general applicability of the charge-transfer complex to simultaneously improve the electrical conductivity and mitigate the shortcomings of existing single-moiety-based organic electrode materials, and opens up an uncharted pathway toward the development of high-performance organic electrode materials via the exploration of various combinations of donor–acceptor monomers with different stoichiometry.

1. Introduction

The development of sustainable and economical energy storage technologies is indispensable to address the increasing demand for renewable energy sources and promotion of the widespread adoption of electric vehicles. Lithium-ion batteries (LIBs) are one of the most widely adopted technologies among available energy storage options because of their high energy and power density with reliable stability [1]. Significant increases in the mass production of LIBs are thus expected in the near future to meet the surging needs for electric vehicles and large-scale energy storage systems. We speculate that if electric vehicles were to grow to make up 10% of the global car market, this change alone would necessitate at least a fourfold increase in the total LIB production worldwide [2]. Nevertheless, the large production of LIBs presents a serious issue in terms of the availability of resources, particularly of the transition metals (*i.e.,* Co or Ni) on which the current LIB chemistry heavily relies. The limited amount of transition metal resources and their concentration in certain countries may potentially result in high and/or unstable LIB production costs [1,3]. In addition, the use of large amounts of transition metals is neither sustainable nor environmentally benign, as their production and/or recycling generate substantial carbon dioxide emissions [1,4].

Organic redox compounds have been proposed as promising alternatives to transition-metal-oxide electrode materials in LIBs because of their low cost and earth abundancy as well as the minimal carbon dioxide footprint associated with their synthesis and recycling processes [5–7]. Moreover, whereas the theoretical limit of the charge capacity for conventional electrodes based on transition metal oxides has almost been reached, leaving little room for further improvement, the chemical diversity of organic redox compounds and their light weight offer great

* Corresponding author. Department of Materials Science and Engineering, Research Institute of Advanced Materials (RIAM), Seoul National University, 1 Gwanak-ro, Gwanak-gu, Seoul 08826, Republic of Korea.
E-mail address: matlgen1@snu.ac.kr (K. Kang).
[1] Lead contact.

https://doi.org/10.1016/j.ensm.2019.05.001
Received 30 April 2019; Accepted 1 May 2019
Available online 10 May 2019

promise for further development of high-capacity organic electrodes. For example, some organic compounds such as benzoquinone, rhodizonate, and muconate have been demonstrated to be capable of delivering a specific capacity of 500–600 mAh g^{-1} near 3 V (*vs.* Li/Li^+), which is hardly achievable using conventional transition-metal-oxide-based chemistries [7–9]. Nevertheless, key bottlenecks to further progress include their intrinsically low electrical conductivity and high solubility in organic solvents [6,10,11]. The early developed redox-active organic species were highly dissolvable in the electrolyte, inducing severe cycle degradation and thus offsetting the merits of the initial high charge capacity [12,13]. Moreover, the insulating nature of most organic compounds necessitates the use of a large amount of conductive agents in the electrode preparation, which substantially reduces the practical energy density.

Approaches to resolve these issues have generally included polymerization of the redox-active organic monomers or the fabrication of composites using conductive scaffolds. Polymerization can partly mitigate the dissolution issues by anchoring the redox-active parts to an insoluble polymer backbone, resulting in improvement of the capacity retention [14–16]. However, this improvement is often accompanied by a poorer electrical conductivity and an increase in weight after the polymerization because of the addition of the redox-inactive backbone units, leading to deterioration of both the power capability and gravimetric energy density. The synthesis of composites or hybrids of organic electrode materials using conductive scaffolds based on carbonaceous materials has also often been applied [17,18]. The conductive scaffolds enhance the electrical conduction in the electrode and provide anchoring sites for the redox organic compounds, thus improving the power and capacity retention. However, the substantial amount of additional matrices or scaffolds significantly increases the electrode weight, thus reducing the specific energy density. Moreover, the anchoring of the organic compounds is only partially effective for long-term cycling.

Herein, we propose the formation of organic charge-transfer complexes (OCTCs) as a viable self-anchoring approach that can mitigate these issues of reduced electrical conductivity and dissolution, thereby preserving the intrinsic redox capability of organic compounds (Fig. 1). An OCTC is an association of two or more types of organic molecules in which a fraction of electronic charge is transferred between the molecular entities [19,20]. An OCTC generally consists of two types of constituents, an electron-donating and electron-accepting molecule, and any molecule couples with different electron-accepting capabilities are potential OCTC candidates. Constituting molecule couples in OCTCs are typically bound to each other, forming a molecular layer through strong hydrogen bonds and offering high structural stability. In addition, the common π–π interaction between the layers of molecules promotes well-ordered stacking of these molecular layers (Fig. 1a). The dense electron cloud formed in the slab space by the π–π interaction creates a charge-transport path between the layers through which electrons can move freely, resulting in significantly enhanced electrical conductivity compared with that of each constituting molecule unit [19–25]. (Fig. 1b) Fig. 1c comparatively illustrates the electrical conductivities of the OCTCs reported hereafter (phenazine–7,7,8,8-tetracyanoquinodimethane (PNZ–TCNQ) and dibenzo-1,4-dioxin–7,7,8,8-tetracyanoquinodimethane (DD–TCNQ)), with those of the precursor organic materials (phenazine (PNZ), 7,7,8,8-tetracyanoquinodimethane (TCNQ), and dibenzo-1,4-dioxin (DD)), demonstrating the orders-of-magnitude enhancement. Notably, the electrical conductivity of the OCTCs is even comparable to those of commercialized cathode materials such as $LiMn_2O_4$, NCM111 ($LiNi_{1/3}Co_{1/3}Mn_{1/3}O_2$), and $LiFePO_4$ [19,26–30]. Because of their unique material properties distinct from other organic compounds, OCTCs have been applied as semiconductors [31] and superconductors [32]; however, they have not yet been investigated for use in rechargeable batteries. While some metal-organic compounds such as Cu-TCNQ have been explored to enhance the intrinsic property of organic electrodes (*e.g.* TCNQ) in batteries, synergetic effects of both organic constituents in the OCTC remain elusive [33,34]. In the following, we provide two examples of newly developed OCTCs that can serve as promising positive electrodes for lithium rechargeable batteries. In the first example, a new OCTC is constructed from two well-known redox active species with different electron affinities, and its feasibility as a positive electrode material in a lithium cell is examined. Subsequently, the OCTC is modified using a new high-voltage p-type redox active moiety as an electron-donating molecule to demonstrate the high energy density achievable with full utilization of the OCTC constituents.

2. Results and discussion

2.1. Structure and performances of PNZ–TCNQ

PNZ [35] and TCNQ [36] are some of the most widely studied redox active organic compounds and were selected as the first model constituents for the formation of the new OCTC electrode [22,37]. (Fig. 2a) PNZ and TCNQ have been previously reported as potential electrode materials for LIBs, which can deliver redox activity at 1.5/1.2 V and 3.2/2.6 V (*vs.* Li/Li^+), respectively. Nevertheless, their low electrical conductivities and their dissolution in the electrolyte lead to low power capability and poor cycle stability [35,36]. Although the redox potential of PNZ is relatively low and inadequate for its use as the positive electrode, the planar structures of PNZ were expected to aid in inducing a well-defined layered crystalline structure with TCNQ in the formation of the OCTC [19]. As

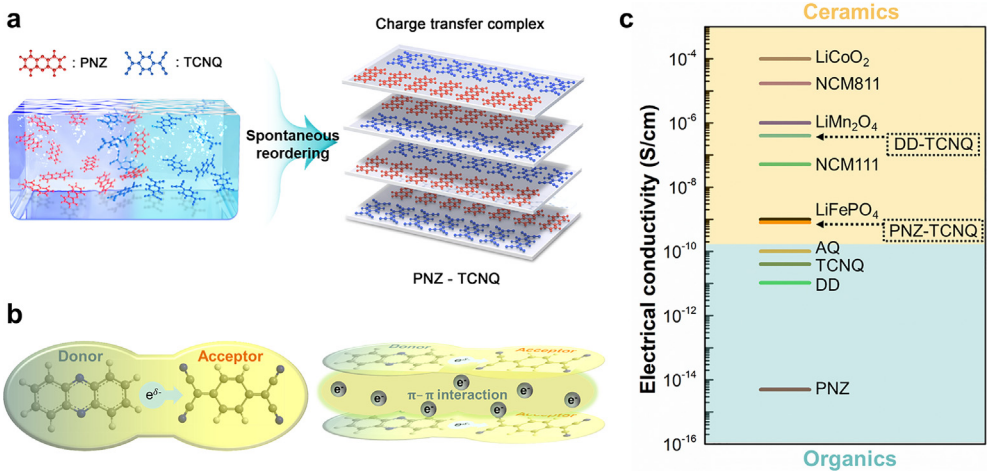

Fig. 1. Concepts of organic charge-transfer complex (OCTC). (a) Conceptual diagram and brief structural description of the OCTC PNZ–TCNQ. (b) Schematic diagram of working principles of the OCTC. (c) Electrical conductivities of representative inorganic and organic redox active species and OCTCs.

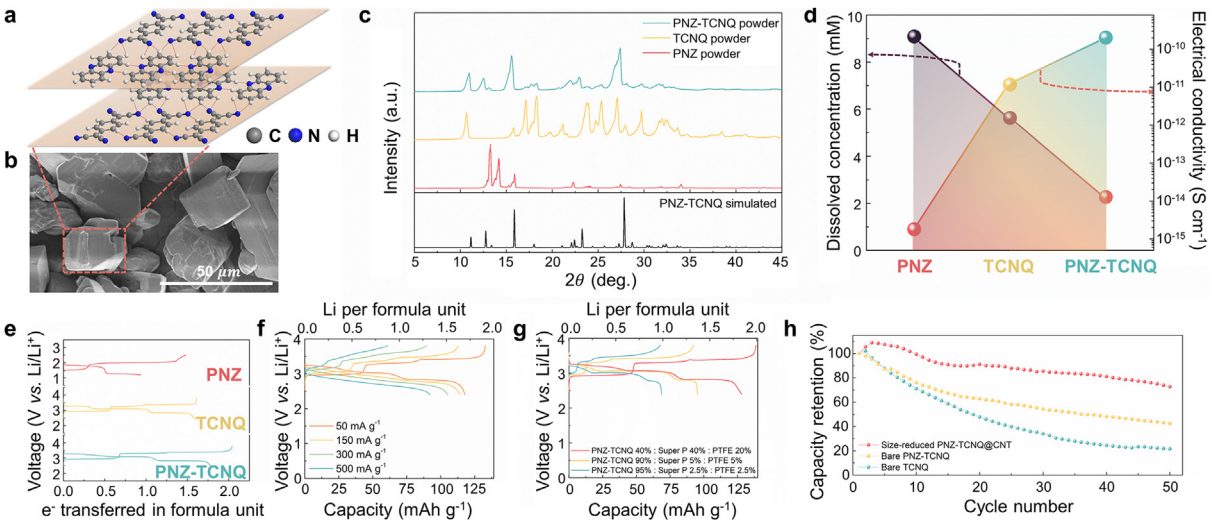

Fig. 2. Material characterization and electrochemical performances of PNZ–TCNQ. (a) Detailed structural information for PNZ–TCNQ. (dotted line: hydrogen bonds between molecules, **π–π** interactions occur between the slabs). (b) SEM image of pristine PNZ–TCNQ powder. (c) XRD patterns of PNZ–TCNQ, monomer units, and simulated PNZ–TCNQ. (d) Material properties of PNZ, TCNQ, and PNZ–TCNQ. Solubility with electrolytes measured using UV–vis spectroscopy after 6-h storage at high temperature (60 °C). The electrical conductivities were determined using four-probe measurements (See also Fig. S1). (e) Voltage–capacity profiles of monomolecules (PNZ, TCNQ) and charge-transfer complex (PNZ–TCNQ) during the second cycle (See also Fig. S2). (f) Rate capability of PNZ–TCNQ at 50, 150, 300, and 500 mA g^{-1}. (g) Voltage–capacity profiles with high contents of active materials: 40 *wt*%, 90 *wt*%, and 95 *wt*% in total electrode. (h) Capacity retention curves of bare TCNQ, bare PNZ–TCNQ, and size-reduced PNZ–TCNQ aligned on CNTs (See also Figs. S3 and S4).

such, the OCTC based on PNZ–TCNQ was prepared from a simple mixing process at room temperature. The PNZ and TCNQ powders were mixed/stirred in acetone solvent in an equimolar ratio at room temperature for 3 h followed by vacuum filtration and drying at 30 °C overnight. Characterization of the resultant powder indicated that the PNZ–TCNQ OCTC was successfully obtained via this single-step reaction. Well-defined cubic particles are clearly observable in the scanning electron microscopy (SEM) images in Fig. 2b, suggesting the formation of a new crystalline phase after the mixing and drying processes. The X–ray diffraction (XRD) patterns in Fig. 2c further elucidate that the structure of the OCTC differs from that of the starting materials of PNZ and TCNQ and is consistent with the simulated XRD pattern based on an ordered layered structure of a PNZ–TCNQ OCTC [37]. According to the structural model, all of the molecules are connected in a single layer by bondings between nitrogen and hydrogen atoms in PNZ and TCNQ (Fig. 2a). [37] It is also noted that the π–π attractive force aids in maintaining the well-ordered stacking of the layers as the π–π conjugation field can be built up between the layers [19,24,25]. The presence of the strong intermolecular forces between the molecular entities is believed to aid in the facile room-temperature synthesis of PNZ–TCNQ OCTC with high yield and contribute to the stability of the crystal structure.

Fig. 2d compares the intrinsic material properties of the OCTC with those of PNZ and TCNQ. The electrical conductivity of the OCTC (8×10^{-10} S cm^{-1}) was 10^5 and 20 times higher than those of PNZ and TCNQ, respectively [38,39], and represents remarkably high electrical conductivities among redox active organic materials reported (Fig. 1c). This notable enhancement of the electrical conductivity after the formation of the OCTC agrees with the general observation for charge-transfer complexes that the structural aspect involving the π–π interaction in the slab space typically results in the formation of a fast charge-transport path [24,25]. In addition, ultraviolet–visible (UV–vis) spectroscopy analysis revealed that the dissolution of the OCTC was notably reduced compared with those of its precursor forms. Whereas the PNZ and TCNQ exhibited 9.1 and 5.6 mM solubility in tetraethylene glycol dimethyl ether (TEGDME) solvent after 6-h storage at 60 °C (Fig. 2d, Fig. S1), the OCTC was much more tolerant to the dissolution (2.3 mM solubility). The suppressed dissolution is mainly attributed to the strong intermolecular interaction in the OCTC and resulting large molecular matrix compared with those of the precursor molecules [40,41].

Preliminary electrochemical tests of the OCTC electrode were performed, and the second charge and discharge profiles of the PNZ, TCNQ, and PNZ–TCNQ OCTC electrodes in a lithium half-cell are shown in Fig. 2e and Fig. S2. Considering the theoretical capacities of PNZ and TCNQ (uptake of two lithium per formula unit), the PNZ and TCNQ electrodes retained approximately 50% and 75% of their theoretical capacities, respectively, at a current rate of 50 mA g^{-1}. This result partly agrees with previous reports of PNZ and TCNQ exhibiting relatively low capacities, which were attributed to their insulating nature [35,36]. However, at the same current rate, the OCTC electrode exhibited ~90% of the theoretical capacity. Although the cut-off voltage of the OCTC electrode was limited above 2 V and, thus, the PNZ part in the OCTC remained electrochemically inactive, the activity of the TCNQ part in the complex was notably enhanced [42,43]. (See Fig. S3 for cycle data with the extended lower voltage cut-off.) Fig. 2f further supports the noteworthy improvement in the rate capability of the OCTC. The electrochemical profiles of the OCTC electrode at various current rates illustrate that the retention of the specific capacity was relatively stable even with the current density increase from 20 to 500 mA g^{-1}. The OCTC electrode exhibited ~73% capacity utilization at a current rate of 500 mA g^{-1} compared with that at 50 mA g^{-1}, corresponding to a capacity of 98 mAh g^{-1}. This rate performance is remarkable considering the large particle sizes (~30 μm) of the OCTC in the electrode.

It should be noted that organic electrodes conventionally utilize a low active material content in the electrode (20%–60%) to compensate for the poor electrical conductivity [5–7]. In this respect, we also examined the electrode performance of the OCTC with various conductive carbon contents. Fig. 2g presents the charge and discharge profiles of the OCTC electrodes with three representative carbon contents. As the carbon content decreased, the capacity of the OCTC electrode gradually decreased; however, the electrodes with 90 *wt*% and 95 *wt*% of active material could still deliver approximately 65% and 50% of the theoretical capacity, respectively. Most organic electrodes with such high active material contents and large particle sizes rarely exhibit electrochemical activity under these operating conditions [8,44,45]. The cycle performances of the electrodes were further investigated, as shown in Fig. 2h

and Fig. S4. The OCTC electrode generally displayed improved capacity retention compared with those of the PNZ and TCNQ electrodes. The capacity retention of the OCTC electrode after 50 cycles was 43%, which is substantially higher than that of the TCNQ electrode (21%).

PNZ–TCNQ OCTC showed the relatively higher capacity retention, however, there still exists capacity fading considered to be originated from continuous dissolution, low persistence of oxidized organics or another factor. First, it is speculated that it was not sufficient to sustain the stable cycling in the given electrolyte system from the ex-situ UV–vis spectral analysis (See Fig. S9 for more details). It is observed that the peak intensities of samples in the different state-of-charge are roughly similar, implying that the dissolution properties of the OCTCs at partially charged states are not significantly different from the pristine states. Nevertheless, it also indicated that small amount of dissolution is continuously observed regardless of the state-of-the charges, which may contribute cumulatively to the degradation of the capacity. Furthermore, post mortem analysis of the electrodes using FTIR in Fig. S10 exhibited that the pristine PNZ–TCNQ was chemically stable after cycling, indicating no chemical degradation during charge/discharge processes. Nevertheless, the overall cycle performance requires further improvement, which might be attributed to the unusually large particle size (Fig. 2b) and small amount of dissolution still observed in the OCTC (Fig. 2d). Particle size reduction and additional anchoring to a carbon nanotube (CNT) scaffold could further improve the capacity retention, and the OCTC electrode exhibited enhanced cycle stability, displaying 73% of the capacity after 50 cycles, and thus outperforming the TCNQ and PNZ electrodes [46,47]. While more efforts need to be placed in improving the cycle stability of these TCNQ derivatives in general, it clearly verifies that the charge-transfer complex formation enhances the cycle retention compared with those of its constituting respective organic molecules.

2.2. Strategy for enhancing the energy density

Although improved rate performance with acceptable cycle stability was successfully demonstrated by forming the OCTC from the PNZ and TCNQ, the electrochemical activity of the OCTC was displayed only from the TCNQ redox center. This phenomenon occurred simply because the redox potential of PNZ was too low to be exhibited in the positive electrode voltage window with the cut-off of 2 V (*vs.* Li/Li^+). Moreover, an attempt to discharge to lower voltage ~1 V (*vs.* Li/Li^+) to utilize the PNZ part in the complex induced side reactions in the electrochemical cell [43,48]. Thus, we redesigned the OCTC by considering potential organic compounds that are capable of delivering high redox voltages while also exhibiting an electron-donating nature to form a charge-transfer complex with the electron-accepting TCNQ. This combination would enable the new OCTC to display the electrochemical activities from both constituting molecules with an expected enhanced energy density. In our search for a counterpart to TCNQ, we identified dibenzo–1,4–dioxin (DD) as a new high-potential p-type redox organic compound. Our preliminary electrochemical test of a DD electrode revealed that a reversible redox reaction occurs at approximately 4.2 V (*vs.* Li/Li^+) in the lithium cell (Fig. S5). Moreover, the planar molecular structure of DD, as depicted in Fig. 3a, was expected to be beneficial for the formation of the OCTC with TCNQ. Following a similar mixing process as that used in the previous PNZ–TCNQ OCTC synthesis, we succeeded in fabricating a new OCTC based on DD (an electron donor) and TCNQ (an electron acceptor) at room temperature.

2.3. Material and electrochemical properties of DD–TCNQ

The structural analysis supports that the OCTC was successfully prepared from DD and TCNQ. The SEM image in Fig. 3b confirms that well-ordered platelet particles were formed after the synthesis, and the XRD

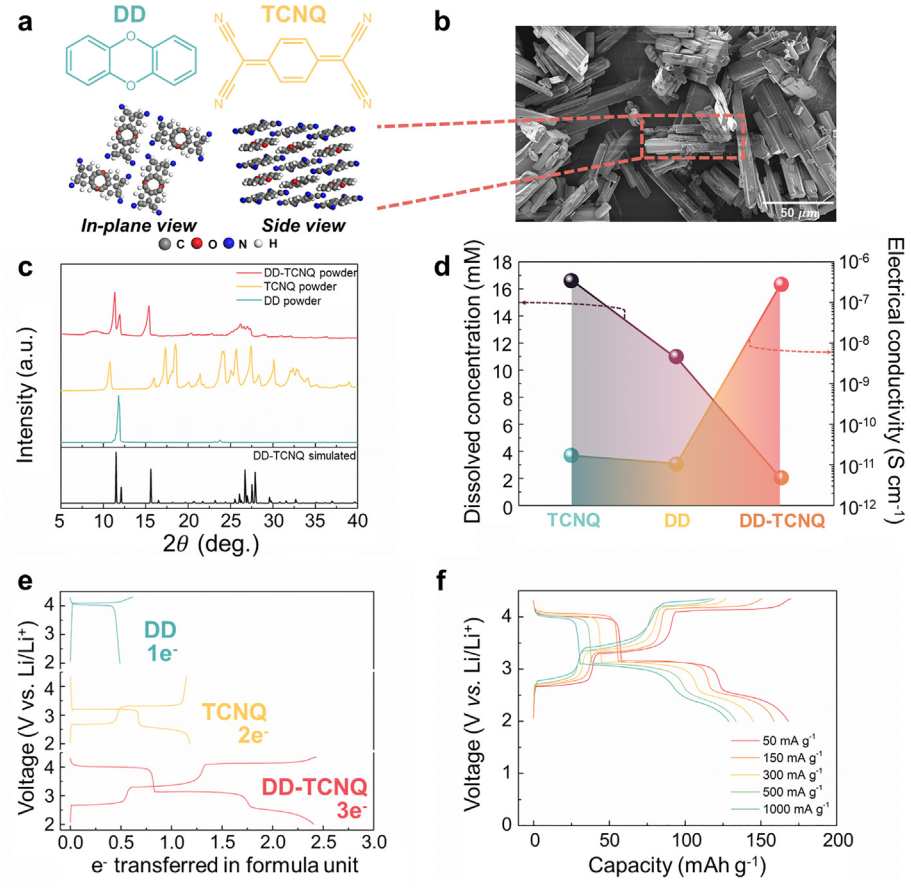

Fig. 3. Material properties and electrochemical performances of DD–TCNQ. (a) Chemical formula of DD and TCNQ and detailed structural information for DD–TCNQ: in-plane and side view (**π–π** interactions occur between the slabs). (b) SEM image of pristine DD–TCNQ powder. (c) XRD patterns of DD–TCNQ and its monomers and simulated pattern of DD–TCNQ. (d) Material properties of DD, TCNQ, and DD–TCNQ. Solubility with electrolytes measured using UV–vis spectroscopy after 6-h storage at high temperature (60 °C). The electrical conductivities were determined using four-probe measurements. (e) Voltage–capacity profiles of monomolecules (DD, TCNQ) and charge–-transfer complex (DD–TCNQ) during the second cycle (See also Fig. S7). (f) Rate capability of DD–TCNQ at 50, 150, 300, 500, and 1000 mA g^{-1} (See also Figs. S5, S6, S8, S9, and S10).

pattern of the obtained powder displays a diffraction pattern matched with the simulated pattern and is distinct from those of its precursors, as shown in Fig. 3c [49]. The structural merits of the OCTC were consistently observed for the DD–TCNQ OCTC as well. Furthermore, it is observed that the chemical states of each constituting monomers are well-preserved as presented from the series of UV–Vis spectra (Fig. S6). The UV–Vis spectra of charge transfer complexes are consistent with those of constituents, indicating the formation of the complex from the precursor moieties without any side reactions. Fig. 3d illustrates that the electrical conductivity increased remarkably with the formation of the DD–TCNQ OCTC to 2.785×10^{-7} S cm^{-1}, which is more than 10^4 times greater than that of DD and TCNQ and is even higher than that of the PNZ–TCNQ complex. Notably, this value is comparable to those of conventional transition-metal-oxide-based electrode materials such as $LiMn_2O_4$ and $LiNi_{1/3}Co_{1/3}Mn_{1/3}O_2$ [28,29]. The solubility test in ethylene carbonate/dimethyl carbonate (EC/DMC) solvent for 6 h at 60 °C revealed that the dissolution of DD and TCNQ could also be simultaneously suppressed (Fig. 3d). The DD–TCNQ OCTC exhibited a low solubility (2 mM) that was more than 5 and 8 times lower than that of DD (11 mM) and TCNQ (16.6 mM), respectively, under the same conditions.

The electrochemical properties of the DD–TCNQ OCTC electrode in a lithium cell were investigated to examine the change in the energy density and rate capability corresponding to the improved material properties. Fig. 3e shows that the DD–TCNQ OCTC clearly exhibited the electrochemical activity of both DD and TCNQ at ~4.2 V and ~(3.2/2.6) V (*vs.* Li/Li$^+$), respectively. Moreover, the complex utilizes a three-electron redox reaction from both the DD and TCNQ units in the structure, which is equivalent to the theoretical specific capacity of 207 mAh g^{-1} and theoretical energy density of 683 Wh kg^{-1} (when paired with Li metal and considering only the mass of the working electrode) (Fig. S7). We observed that the high energy density of the new OCTC could also be retained at high current rates, as depicted in Fig. 3f. Even at a current rate of 1000 mA g^{-1}, both the charge and discharge capacity could be stably maintained, delivering a specific capacity of 130 mAh g^{-1}, which corresponds to 76% of the capacity at 50 mA g^{-1}. Nevertheless, DD–TCNQ OCTC exhibited a relatively low cycle retention, which warrants further study to optimize it. (Fig. S8). As DD electrode alone could not be cycled at all in the same electrolyte condition due to its severe dissolution problem, it is speculated that, while the dissolution of DD was mitigated in the form of DD-TCNQ, it was not sufficient to sustain the extended cycle in the given electrolyte system (See Fig. S9 for more details). Regarding the intrinsic chemical stability of the electrode during cycles, post mortem analysis of the electrodes using FTIR were additionally carried out as shown in Fig. S10. It revealed that the pristine DD-TCNQ chemical structure was stably maintained after cycling, implying that the major origin of the capacity fade is not likely to be the thermodynamic instability of the electrode at different charging states.

2.4. Redox mechanism of DD–TCNQ

To verify the redox mechanism of this new organic electrode, the lithium cells were disassembled during charge and discharge at different states-of-charge and analyzed. The charge/discharge protocol was set to firstly discharge the electrode to 2.2 V *vs.* Li/Li$^+$, and then charged and re-discharged within 4.3–2.2 V. The electrochemical cycle and the corresponding analysis presented in Fig. 4 begins with the fully discharged state of DD–TCNQ, DD-Li_2TCNQ, followed by the charge and re-discharge. Fig. 4 shows the *ex situ* Fourier–transform infrared (FTIR) spectroscopy spectra and X–ray photoelectron spectroscopy (XPS) spectra at each end of the voltage plateaus during the second cycle. The FTIR spectra in Fig. 4b illustrates the negative shift of C≡N stretching and its splitting into two peaks at 2200 cm^{-1} and 2180 cm^{-1} during discharge below the 4-V region, which are restored during the charge

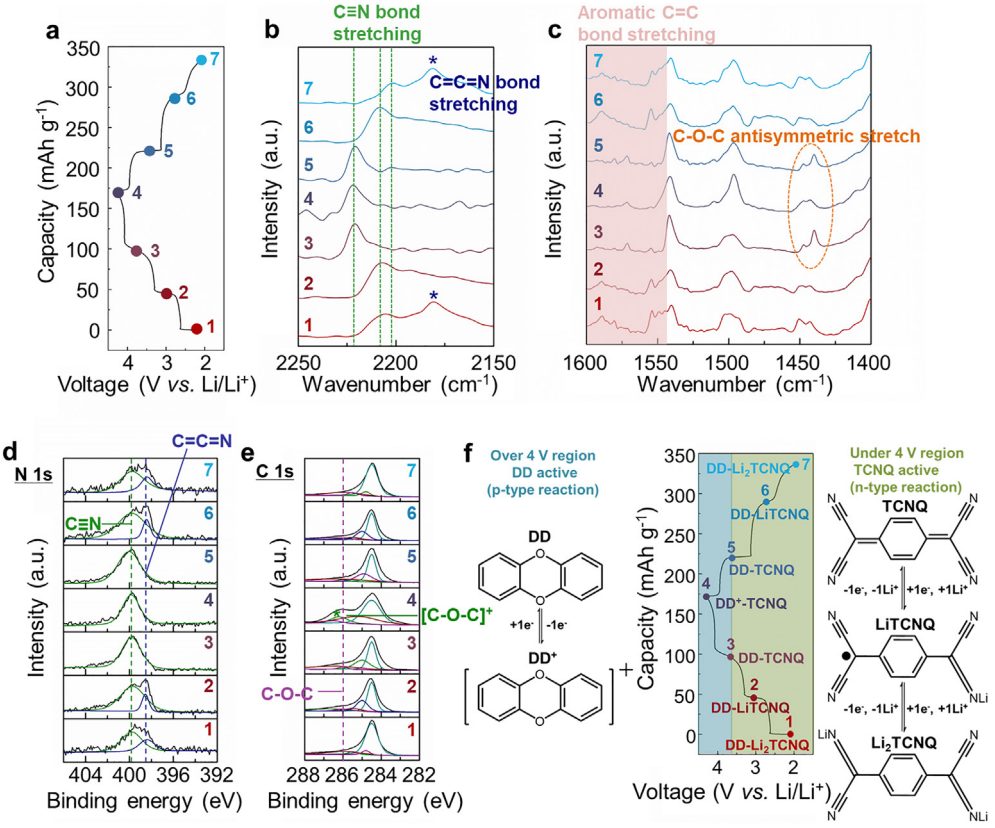

Fig. 4. Investigation of redox mechanism of DD–TCNQ. (a) Voltage–capacity profile of DD–TCNQ. *Ex situ* FTIR data in the regions of (b) 2250–2150 cm^{-1} and (c) 1600–1200 cm^{-1}. *Ex situ* XPS data in the regions of (d) 406–392 eV and (e) 288–282 eV. (f) Suggested redox mechanism of DD–TCNQ (See also Fig. S11).

(from state 4 to state 7 in Fig. 4). Nitrile bond breaks down to double bond after that nitrogen atom gets an electron (and a lithium ion) during discharge, and the neighboring C–C bond becomes a double bond. During charge to 4 V, the peaks positively shifted back to its original wavenumber (~2225 cm^{-1}), indicating the recovery of the nitrile bond of the TCNQ unit. However, the reverse behavior was observed during discharge, which is attributed to the lithium insertion accompanying the reduction in the C≡N triple bond and suggests that the main redox reaction below 4 V occurs at the TCNQ part in the complex. This observation also agrees with the previously reported redox mechanism of TCNQ, which indicates that TCNQ follows a reversible aromatization mechanism [36]. In contrast, a notable change in the C–O–C vibration at 1280 cm^{-1} was observed above 4 V, as indicated by the dotted circle in Fig. 4c. The generally positive shift of the C–O–C vibration suggests that the oxidation occurs near the C–O–C bond in the DD part, identifying this moiety as the redox center in the complex above 4 V.

A more detailed picture of the redox mechanism can be obtained from the XPS results in Fig. 4d and e. The N 1s spectra in Fig. 4d shows that the ratio of the two peaks centered at 399.9 and 398.5 eV, corresponding to C≡N and C=C=N groups in the as-prepared electrode, respectively, reversibly changes, where the C=C=N peak gradually disappears with charging and reappears with discharging. Notably, the change in the C=C=N peak is not observed above 4 V, indicating the absence of the redox reaction of TCNQ. The C 1s spectra in Fig. 4e, however, offers information on the redox activity above 4 V. It is clear that the C^{+}–O–C peak at 286.2 eV emerges significantly with charging and disappears upon discharge above the 4-V region. In addition, the C–O–C peak (286.0 eV) slightly shifts to the C^{+}–O–C peak at 286.2 eV, which is consistent with the FTIR result and confirms that the redox activity is centered at C–O–C in the DD part of the complex. Nevertheless, we only observed a negligible change in the O 1s peak, which is not fully understood and requires more detailed analysis of the redox mechanism of DD (Fig. S11). The current spectroscopy results suggest that DD undergoes a single-electron redox reaction above the 4-V region, whereas TCNQ undergoes a two-electron redox reaction below the 4-V region during battery cycling. At each stage of charge and discharge, it is proposed that the original state of the DD–TCNQ OCTC transforms to DD–LiTCNQ, DD–Li_2TCNQ, and DD^{+}–TCNQ, as denoted in Fig. 4f. It can be summarized that the DD in the OCTC has an anion uptake/loss with p-type redox, and on the other hand, TCNQ in the OCTC participates an n-type redox reaction with a lithium uptake/loss. The detailed redox mechanism of DD–TCNQ is illustrated in equation (1).

$$DD-TCNQ \longrightarrow DD-Li_2TCNQ \underset{Discharge\ to\ 2V}{\overset{Charge\ to\ 4V}{\rightleftarrows}} DD-TCNQ \underset{Discharge\ to\ 4V}{\overset{Charge\ to\ 4.3V}{\rightleftarrows}} DD^{+}TFSI^{-}-TCNQ \quad (1)$$

Equation 1. Suggested redox mechanism of DD–TCNQ.

These series of observations confirm that DD and TCNQ, the constituents of the DD–TCNQ OCTC, fully participate in the redox reaction, resulting in the enhanced energy density of the OCTC. Furthermore, the formation of the OCTC is proposed as a viable approach to combine the electrochemical activities of the two different organic redox compounds into one structure with the additional benefits of enhanced electrical conductivity and structural stability.

3. Conclusion

In summary, we demonstrated the use of a charge-transfer complex as a novel type of organic electrode material for the first time. The formation of OCTCs from various organic redox compounds potentially results in several advantages for electrode materials in rechargeable battery chemistries. Because of the general structural characteristics of the charge-transfer complex, the electrical conductivity and structural integrity can be greatly improved. In particular, the electrical conductivity of the suggested OCTC (DD–TCNQ) exhibit remarkable high value among organic electrode materials reported to date and is comparable to that of transition-metal-oxide-based electrode materials. The achievement of a large energy density by combining two redox moieties in the OCTC can lead to a large practical energy density, ~560 Wh kg^{-1} corresponding to 82% of the theoretical value, for the DD–TCNQ electrode. (when paired with Li metal and considering only the mass of the working electrode). Even at a high current rate and using practical electrode formulation ratios, the new OCTC electrode retained respectable power and cycle performance. Various combinations of organic redox-active molecules can be considered for OCTCs to exploit different electron-accepting capabilities. Therefore, the integration of the distinct advantages of each organic redox-active moiety is expected to be possible by applying the charge-transfer complex strategy, resulting in improved electrical and structural properties. The electrochemical performance of the OCTCs reported in this work, PNZ–TCNQ and DD–TCNQ OCTC, is not yet comparable to that of currently used inorganic-based electrode materials. It is believed that to optimize the electrochemical performances, one need to further find the highly compatible electrolytes or utilize the conductive scaffold such as CNT and graphene. As various combinations of organic moieties are possible to construct the organic charge transfer complexes, more appropriate material candidates in organic charge transfer complexes which can better solve the dissolution and conductivity problems at the same time can be explored in the further work. The feasible formation of OCTCs from any molecule couples with different electron-accepting capabilities along with a future fundamental study on this new chemistry suggests the great promise for new organic electrode discovery via the exploration of numerous combinations of organic redox-active species. Moreover, the simple synthetic process of OCTCs via co-precipitation of two or more types of organic molecules in solvents at moderate temperature can offer additional merits.

3.1. Experimental procedures

3.1.1. Preparation of materials

PNZ and DD were purchased from Alfa Aesar (USA), and TCNQ was purchased from Sigma-Aldrich (UK). All the commercially available chemicals were utilized without further purification. The charge-transfer complexes, PNZ–TCNQ and DD–TCNQ, were synthesized following a procedure previously described in the literature [34,46]. The PNZ and TCNQ powders were mixed in an equimolar ratio in acetone solvent for 3 h at room temperature. The resulting solution was filtered, and the residue was dried at 30 °C overnight. The DD and TCNQ powders were mixed in an equimolar ratio in acetonitrile solvent for 30 min at room temperature, and the resulting solution was dried at 30 °C for 3 h.

3.2. Material characterization

XRD profiles of the powder samples of PNZ–TCNQ and its monomers were characterized using a D2 PHASER (Bruker, Bremen, Germany) equipped with Cu-Kα radiation (λ= 1.54178 Å) at a scanning speed of 0.2° min^{-1} in the 2θ range of 5°–60°. The electrolytes with the stored electrode samples were characterized using a UV–vis spectrometer (Agilent Technologies, Cary 5000) with an optical glass cuvette (Quartz;

Hellma®). The fabricated electrodes of the PNZ–TCNQ series (PNZ–TCNQ and its monomer units) and DD–TCNQ series (DD–TCNQ and its monomer units) were stored in the electrolytes (1 M LiTFSI in TEGDME and 5 M LiClO4 in EC/DMC (v/v = 1:1)) for 6 h at 60 °C. A lab-made four-probe station with an Agilent 4156C semiconductor parameter analyzer was used to measure the electrical conductivities of the charge-transfer complexes and their constituting monomers. To evaluate the electrical conductivities, pelletized powders were prepared with thicknesses of ~3 mm.

3.3. Electrochemical measurements

Voltage–capacity profiles of the charge-transfer complexes and their constituting molecules versus a Li metal foil (Hohsen, Japan) in coin-type cells (CR2032) were obtained. The Li metal anode was prepared in an Ar-filled glove box. The cathodes were fabricated by mixing 40% w/w active materials, 40% w/w carbon black (Super P), and 20% w/w polytetrafluoroethylene (PTFE, Aldrich) binder, and all of the sampled-electrodes are 4–6 mg. Especially for the high-content test, cathodes with two additional compositions were formulated by mixing 90% w/w active materials, 5% w/w carbon black, and 5% w/w PTFE binder and 95% w/w active materials, 2.5% w/w carbon black, and 2.5% w/w PTFE binder. A porous glass microfiber membrane (GF/F; Whatman, UK) was used as a separator in the Li cells. The electrolytes were 1 M LiTFSI in TEGDME for PNZ–TCNQ and 5 M $LiClO_4$ in EC/DMC for DD–TCNQ, and the cells were assembled in an inert atmosphere within an Ar-filled glove box. The electrochemical measurements were performed at a constant current density of 50 mA g^{-1} in the voltage range of 2.4–3.8 V and 2.4–4.3 V *vs.* Li/Li^+ for PNZ–TCNQ and DD–TCNQ, respectively, using a battery test system (Won-A Tech, Korea).

3.4. Ex situ electrode characterization

The electrodes of PNZ–TCNQ and TCNQ at different states of cycling were prepared by disassembling coin cells (pristine, 2 cycles, 10 cycles, and 50 cycles) followed by rinsing the electrodes with TEGDME. XRD profiles were obtained using the D2 PHASER with Cu-Kα radiation (λ= 1.54178 Å) at a scanning speed of 0.2° min^{-1} in the 2θ range of 5°–60°. The surface morphologies of the electrodes were examined using SEM (MERLIN Compact, ZEISS, Germany). XPS measurements were performed using an Axis Supra™ from Kratos (U.K.). All the measured spectra were set to the reference of C 1s (284.4 eV), which is correlated to the Super P. FTIR spectra were measured using pellets made of the electrodes at different states and KBr powder on an FT/IR-4200 (Jasco, Japan) at a resolution of 4 cm^{-1}. UV–vis spectra measurements were performed using an JASCO-3000 (Jasco, Japan) at a resolution of 10 nm.

3.5. Size reduction of particles of PNZ–TCNQ and synthesis of CNT aligned electrodes

Size reduction of the PNZ–TCNQ particles was performed using an anti-solvent reduction method. The PNZ–TCNQ powder was dissolved in distilled water to obtain a saturated solution. Then, the same amount of anti-solvent (acetone) was added to the saturated solution followed by 10 min of sonication. The resulting solution was filtered, and the residue was dried overnight at 30 °C in a vacuum oven. CNT aligned electrodes were synthesized, followed by mixing the CNTs (5 mg) and PNZ–TCNQ (5 mg) in the acetone solvent (20 mL). The solution was homogenized using an ultrasonic Vibra Cell VCX 750 homogenizer (Sonics & Materials Inc., USA) for 10 min (2-s on, 1-s off). The resulting solution was also filtered, and the residue was dried overnight at 30 °C in a vacuum oven.

Author contributions

S.L. J.H. and K.K. planned the project. K.K. supervised all aspects of the research. S.L. designed, synthesized, characterized, and electrochemically tested the suggested materials. J.H. designed and promoted the overall progress of the research with S.L. S.-K.J. K. Ku contributed data for the material properties with S.L. G.K. suggested and developed the further strategy for enhancing the energy density with substituting other material with S.L. W.M.S. and I. K. acquired the SEM data with input from S.L. H.K. performed and analyzed XRD data with S.L. G.Y. contributed to design the figure legend of structural details with S.L. K.H. acquired the electrical conductivity data with the supervision of H.W.J. The manuscript was written by S.L. and was revised by J.H. S.-K.J. and K. Ku. All of the authors commented and discussed for the manuscript.

Declaration of interests

The authors declare no competing interests.

Acknowledgement

This research was supported by Creative Materials Discovery Program through the National Research Foundation of Korea (NRF) funded by the Ministry of Science, ICT and Future Planning (NRF-2017M3D1A1039553). This work was supported by the National Research Foundation of Korea(NRF) grand funded by the Korea government(MSIP) (No. 2015R1A2A1A10055991).

Appendix A. Supplementary data

Supplementary data to this article can be found online at https://doi.org/10.1016/j.ensm.2019.05.001.

References

[1] J.M. Tarascon, M. Armand, Issues and challenges facing rechargeable lithium batteries, Nature 414 (2001) 359–367.
[2] B. Lee, K. Kang, Materials science: long-lived electrodes for plastic batteries, Nature 549 (2017) 339–340.
[3] D. Larcher, J.-M. Tarascon, Towards greener and more sustainable batteries for electrical energy storage, Nat. Chem. 7 (2015) 19–29.
[4] M. Armand, J.-M. Tarascon, Building better batteries, Nature 451 (2008) 652–657.
[5] Y. Liang, Z. Tao, J. Chen, Organic electrode materials for rechargeable lithium batteries, Adv. Energy Mater. 2 (2012) 742–769.
[6] S. Lee, K. Giyun, K. Kyojin, Y. Kyungho, J. Sung-Kyun, L. Hee-Dae, K. Kisuk, Recent progress in organic electrodes for Li and Na rechargeable batteries, Adv. Mater. 30 (2018) 1704682.
[7] Z. Song, H. Zhou, Towards sustainable and versatile energy storage devices: an overview of organic electrode materials, Energy Environ. Sci. 6 (2013) 2280–2301.
[8] T.B. Schon, B.T. McAllister, P.-F. Li, D.S. Seferos, The rise of organic electrode materials for energy storage, Chem. Soc. Rev. 45 (2016) 6345–6404.
[9] M. Lee, et al., High-performance sodium–organic battery by realizing four-sodium storage in disodium rhodizonate, Nat. Energy 2 (2017) 861–868.
[10] M. Lee, H. Jihyun, S. Dong-Hwa, N. Dong Heon, N. Ki Tae, K. Kisuk, Redox cofactor from biological energy transduction as molecularly tunable energy-storage compound, Angew. Chem. Int. Ed. 125 (2013) 8480–8486.
[11] X. Wu, et al., Unraveling the storage mechanism in organic carbonyl electrodes for sodium-ion batteries, Sci. Adv. 1 (2015), e1500330.
[12] D. Williams, J. Byrne, J. Driscoll, A high energy density lithium/dichloroisocyanuric acid battery system, J. Electrochem. Soc. 116 (1969) 2–4.
[13] H. Senoh, M. Yao, H. Sakaebe, K. Yasuda, Z. Siroma, A two-compartment cell for using soluble benzoquinone derivatives as active materials in lithium secondary batteries, Electrochim. Acta 56 (2011) 10145–10150.
[14] T. Le Gall, K.H. Reiman, M.C. Grossel, J.R. Owen, Poly (2, 5-dihydroxy-1, 4-benzoquinone-3, 6-methylene): a new organic polymer as positive electrode material for rechargeable lithium batteries, J. Power Sources 119 (2003) 316–320.
[15] Z. Song, H. Zhan, Y. Zhou, Anthraquinone based polymer as high performance cathode material for rechargeable lithium batteries, Chem. Commun. 4 (2009) 448–450.
[16] Z. Song, H. Zhan, Y. Zhou, Polyimides: promising energy-storage materials, Angew. Chem. Int. Ed. 122 (2010) 8622–8626.
[17] W. Choi, S. Ohtani, K. Oyaizu, H. Nishide, K.E. Geckeler, Radical polymer-wrapped SWNTs at a molecular level: high-rate redox mediation through a percolation network for a transparent charge-storage material, Adv. Mater. 23 (2011) 4440–4443.
[18] T. Sukegawa, K. Sato, K. Oyaizu, H. Nishide, Efficient charge transport of a radical polyether/SWCNT composite electrode for an organic radical battery with high charge-storage density, RSC Adv. 5 (2015) 15448–15452.

[19] K.P. Goetz, D. Vermeulen, M.E. Payne, C. Kloc, L.E. McNeli, O.D. Jurchescu, Charge-transfer complexes: new perspectives on an old class of compounds, J. Mater. Chem. C 2 (2014) 3065–3076.
[20] J.B. Torrance, An overview of organic charge-transfer solids: insulators, metals, and the neutral-ionic transition, Mol. Cryst. Liq. Cryst. 126 (1985) 55–67.
[21] J.R. Kirtley, J. Mannhart, Organic electronics: when TTF met TCNQ, Nat. Mater. 7 (2008) 520.
[22] C.K. Sharma, R. Rogers, CH··· X (X= N, O) hydrogen bond-mediated assembly of donors and acceptors: the crystal structures of phenazine complexes with 1, 4-dinitrobenzene and TCNQ, Cryst. Eng. 1 (1998) 139–145.
[23] Z. Soos, H. Keller, W. Moroni, D. Nöthe, Phenazine cation radical salts: charge-transfer complexes with TCNQ, Ann. NY. Acad. Sci. 313 (1978) 442–458.
[24] J.M. Schultz, Properties of Solid Polymeric Materials: Treatise on Materials Science and Technology, vol. 10, Elsevier, 2017.
[25] Y. Qin, J. Zhang, X. Zheng, H. Geng, G. Zhao, X. Wei, W. Hu, Z. Shuai, D. Zhu, Charge-transfer complex crystal based on extended-π-conjugated acceptor and sulfur-bridged annulene: charge-transfer interaction and remarkable high ambipolar transport characteristics, Adv. Mater. 26 (2014) 4093–4099.
[26] A. Aumüller, E. Hädicke, S. Hünig, A. Schätzle, J.U. von Schütz, Crystal structure and conductivity of a novel charge-transfer complex of N, N′-Dicyano-1, 4-naphthoquinonediimine and tetrathiafulvalene, Angew. Chem. Int. Ed. 23 (1984) 449–450.
[27] A.L. Sutton, B.F. Abrahams, D.M. D'Alessandro, T.A. Hudson, R. Robson, P.M. Usov, Structural and optical investigations of charge transfer complexes involving the radical anions of TCNQ and F 4 TCNQ, CrystEngComm 18 (2016) 8906–8914.
[28] T.T. Fang, H.Y. Chung, Reassessment of the electronic-conduction behavior above the verwey-like transition of Ni2+-and Al3+-doped LiMn2O4, J. Am. Ceram. Soc. 91 (2008) 342–345.
[29] R. Guo, P. Shi, X. Cheng, Y. Ma, Z. Tan, Effect of Ag additive on the performance of LiNi1/3Co1/3Mn1/3O2 cathode material for lithium ion battery, J. Power Sources 189 (2009) 2–8.
[30] M.S. Whittingham, Lithium batteries and cathode materials, Chem. Rev. 104 (2004) 4271–4302.
[31] S. Horiuchi, T. Hasegawa, Y. Tokura, Molecular donor–acceptor compounds as prospective organic electronics materials, J. Phys. Soc. Jpn. 75 (2006), 051016.
[32] G. Saito, Y. Yoshida, in: Unimolecular and Supramolecular Electronics I, Springer, 2011, pp. 67–126.
[33] J. Ma, E. Zhou, C. Fan, B. Wu, C. Li, Z.H. Lu, J. Li, Endowing CuTCNQ with a new role: a high-capacity cathode for K-ion batteries, Chem. Commun. 54 (2018) 5578–5581.
[34] C. Fang, et al., A metal–organic compound as cathode material with superhigh capacity achieved by reversible cationic and anionic redox chemistry for high-energy sodium-ion batteries, Angew. Chem. Int. Ed. 56 (2017) 6793–6797.
[35] B. Tian, Z. Ding, G.H. Ning, W. Tang, C. Peng, B. Liu, J. Su, C. Su, K.P. Loh, Amino group enhanced phenazine derivatives as electrode materials for lithium storage, Chem. Commun. 53 (2017) 2914–2917.
[36] Y. Hanyu, I. Honma, Rechargeable quasi-solid state lithium battery with organic crystalline cathode, Sci. Rep. 2 (2012) 453.
[37] I. Goldberg, U. Shmueli, Structure and packing arrangement of molecular compounds. III.(1: 1) 7, 7, 8, 8-Tetracyanoquinodimethane–phenazine, Acta. Crystall. A-Struct. 29 (1973) 440–448.
[38] S. Aftergut, G. Brown, Electronic properties of phenazine, Nature 189 (1961) 827–828.
[39] H. Afify, F. Abdel-Kerim, H. Aly, A. Shabaka, The electrical conductance of some alkali-and divalent transition metal TCNQ salts, Z. Naturforsch. A 33 (1978) 344–346.
[40] C. Peng, et al., Reversible multi-electron redox chemistry of π-conjugated N-containing heteroaromatic molecule-based organic cathodes, Nat. Energy 2 (2017) 17074.
[41] D.-H. Yang, Z.-Q. Yao, D. Wu, Y.-H. Zhang, Z. Zhou, X.-H. Bu, Structure-modulated crystalline covalent organic frameworks as high-rate cathodes for Li-ion batteries, J. Mater. Chem. A 4 (2016) 18621–18627.
[42] A. Pei, G. Zheng, F. Shi, Y. Li, Y. Cui, Nanoscale nucleation and growth of electrodeposited lithium metal, Nano Lett. 17 (2017) 1132–1139.
[43] J. Lu, Z. Chen, F. Pan, Y. Cui, K. Amine, High-performance anode materials for rechargeable lithium-ion batteries, Electrochem. Energy Rev. 1 (2018) 35–53.
[44] A. Shimizu, Y. Tsujii, H. Kuramoto, T. Nokami, Y. Inatomi, N. Hojo, J.-i. Yoshida, Nitrogen-Containing polycyclic quinones as cathode materials for lithium-ion batteries with increased voltage, Energy Technol. 2 (2014) 155–158.
[45] T. Yokoji, H. Matsubara, M. Satoh, Rechargeable organic lithium-ion batteries using electron-deficient benzoquinones as positive-electrode materials with high discharge voltages, J. Mater. Chem. A 2 (2014) 19347–19354.
[46] M. Lee, J. Hong, H. Kim, H.-D. Lim, S.B. Cho, K. Kang, C.B. Park, Organic nanohybrids for fast and sustainable energy storage, Adv. Mater. 26 (2014) 2558–2565.
[47] Y. Wang, Y. Ding, L. Pan, Y. Shi, Z. Yue, Y. Shi, G. Yu, Understanding the size-dependent sodium storage properties of Na2C6O6-based organic electrodes for sodium-ion batteries, Nano Lett. 16 (2016) 3329–3334.
[48] Y.-Y. Hu, et al., Origin of additional capacities in metal oxide lithium-ion battery electrodes, Nat. Mater. 12 (2013) 1130–1136.
[49] I. Goldberg, U. Shmueli, Structure and packing arrangement of molecular compounds. II. (1:1) 7,7,8,8-Tetracyanoquinodimethane-dibenzo-p-dioxin, Acta Crystallogr. B 29 (1973) 432–440.